probe angle are given in Fig. 2, and their relation to the whole flowfield is shown in Fig. 3. At the shock, stagnation pressure ratio was determined from the local shock angle obtained from a Schlieren photograph. The angles were measured by fitting a circular arc to the relevant portion of the shock, with the indicated over-all accuracy. The approximate location of the maximum entropy streamline between the shock and the edge of the model could therefore be reconstructed, Fig. 4.

Conclusion

Experimental evidence has been obtained for the location of the max entropy streamline behind the detached curved shock on a supersonic two-dimensional flat face. The results support the idea of an entropy layer for such blunt bodies in which the maximum entropy streamline does not wet the body surface.

References

[1] Swigart, R. J., "Hypersonic Blunt Body Flow Fields at Angle of Attack," *AIAA Journal*, Vol. 2, No. 1, Jan. 1964, pp. 115–117.

[2] Webb, H. G. Jr., Dresser, H. S., Adler, B. K., and Waiter, S. A., "Inverse Solution of Blunt-Body Flowfields at Large Angle of Attack," *AIAA Journal*, Vol. 5, No. 6, June 1967, pp. 1079–1085.

[3] Prosnak, W. J., "The Asymmetric Hypersonic Blunt Body Problem," *Fluid Dynamic Transactions*, Vol. 2., Pergamon Press, New York, 1965, pp. 457–476.

[4] Belotserkovskii, O. M. and Chushkin, P. I., "The Numerical Solution of Problems in Gasdynamics," *Basic Developments in Fluid Dynamics*, Vol. 1, Academic Press, New York, 1965, pp. 55–73.

[5] Archer, R. D., "Fast Solution to Supersonic Plane Flat Faced Blunt Body," *AIAA Journal*, Vol. 10, No. 5, May 1972, pp. 707–708.

[6] Brong, E. A. and Leigh, D. C., "Method of Belotserkovskii for Asymmetric Blunt Body Flows," *AIAA Journal*, Vol. 2, No. 10, Oct. 1964, pp. 1852–1853.

[7] Moretti, G. and Abbott, M., "A Time-Dependent Computational Method for Blunt Body Flows," *AIAA Journal*, Vol. 4, No. 14, Dec. 1966, pp. 2136–2141.

[8] Moretti, G. and Bleich, G., "Three-Dimensional Flow around Blunt Bodies," *AIAA Journal*, Vol. 5, No. 9, Sept. 1967, pp. 1557–1562.

[9] D'Souza, N., Molder, S., and Moretti, G., "Numerical Method for Hypersonic Internal Flow over Blunt Leading Edges and Two Blunt Bodies," *AIAA Journal*, Vol. 10, No. 5, May 1972, pp. 617–622.

[10] Masson, B. S., Taylor, T. D. and Foster, R. M., "Application of Godunov's Method to Blunt Body Calculations," *AIAA Journal*, Vol. 7, No. 4, April 1969, pp. 694–698.

[11] Bryer, D. W. and Pankhurst, R. C., *Pressure-Probe Methods for Determining Wind Speed and Flow Direction*, National Physical Lab., England, 1971.

Calculation of Turbulent Shear Stress in Supersonic Boundary-Layer Flows

CHEN-CHIH SUN* AND MORRIS E. CHILDS†
University of Washington, Seattle, Wash.

Nomenclature

C_f = skin friction coefficient
M = Mach number
P = pressure
r = distance normal to centerline
R = radius of the duct
T_{ij} = total stress tensor
u = time-averaged velocity in primary flow direction
v = time-averaged velocity normal to centerline
x = distance parallel to centerline
y = $R-r$
δ = boundary layer thickness
μ = molecular viscosity
η = y/δ
ρ = time-averaged density
τ = shear stress

Subscripts

e = boundary-layer edge condition
∞ = freestream condition

Superscript

$\langle\ \rangle'$ = time-averaged fluctuation value

Received March 29, 1974; revision received June 21, 1974. This work was supported by NASA Grant NGR-48-002-047 under administration of the Aerodynamics Branch, NASA Ames Research Center.

Index categories: Boundary Layers and Convective Heat Transfer—Turbulent; Supersonic and Hypersonic Flow; Shock Waves and Detonations.

* Research Assistant Professor, Department of Mechanical Engineering. Member AIAA.

† Professor and Chairman, Department of Mechanical Engineering.

Introduction

IN the study of supersonic turbulent boundary-layer flow the turbulent shear stress distribution has always been of great importance and interest. The direct measurement of the turbulent shear stress is, however, quite difficult. A natural alternative is to compute the shear from experimental mean flow data by numerically integrating the momentum equation. Such computations have been performed in recent studies by Bushnell and Morris,[1] Horstman and Owen,[2] and Sturek.[3] This Note describes results obtained by a computational procedure which differs from those previously reported in that integrated mass and momentum flux profiles, and differentials of these integral quantities are used in the computations so that local evaluation of the streamwise velocity gradient is not necessary. The computed results are compared with measured shear stress data obtained by using hot wire anemometer and laser velocimeter techniques in recent studies by Rose and Johnson.[4,5] The measurements of Rose and Johnson were made upstream and downstream of an adiabatic unseparated interaction of an oblique shock wave with the turbulent boundary layer on the flat wall of a two-dimensional, $M_\infty = 2.9$ wind tunnel. The shock wave was generated by a 7° wedge. The turbulence data obtained from the two independent systems of measurement were in reasonably good agreement, indicating that the data should be reliable. The computational procedure developed here is easy to use, and the computed results show reasonably good over-all agreement with those obtained by direct measurement. As would be expected for any method of computing shear stress from mean flow data, the computed values of shear stress are quite sensitive to small differences in mean flow profiles and to simplifying assumptions which may be made in developing the relationships to be used in the computations. The effect of some of these differences on computed shear stress distributions is discussed.

Basic Equations and Boundary Conditions

The time-averaged equations for the conservation of mass and momentum for steady compressible turbulent boundary-layer flow in an axisymmetric channel are, respectively,

$$\frac{\partial}{\partial x}(\rho u)+\frac{\partial}{\partial x}\langle\rho' u'\rangle+\frac{1}{r}\frac{\partial}{\partial r}(r\rho v)+\frac{1}{r}\frac{\partial}{\partial r}(r\langle\rho' v'\rangle)=0 \qquad (1)$$

and

$$\frac{\partial}{\partial x}(\rho u^2)+\frac{1}{r}\frac{\partial}{\partial r}(r\rho uv)=-\frac{\partial P}{\partial x}+\frac{\partial}{\partial x}T_{xx}+\frac{1}{r}\frac{\partial}{\partial r}rT_{rx} \qquad (2)$$

where

$$T_{xx}=(\tau_v)_{xx}-(\rho\langle u'^2\rangle+2u\langle\rho' u'\rangle) \qquad (3)$$

$$T_{rx}=(\tau_v)_{rx}-(\rho\langle u'v'\rangle+u\langle\rho' v'\rangle+v\langle\rho' u'\rangle) \qquad (4)$$

with τ_v representing the viscous stress.

If we assume that $|v\langle\rho' u'\rangle| \ll |\rho\langle u'v'\rangle|$ and $|\partial\langle\rho' u'\rangle/\partial x| \ll |\partial(\rho u)/\partial x|$ and transform to an x-y coordinate system, the

continuity and momentum equations may be combined and integrated in a direction normal to the surface to yield

$$\frac{\tau}{\rho_e u_e^2}\left(1-\eta\frac{\delta}{R}\right)=\frac{C_f}{2}+\left(\frac{d\delta}{dx}+\frac{\delta}{\rho_e u_e^2}\frac{d\rho_e u_e^2}{dx}+\frac{\delta}{R}\frac{dR}{dx}\right)\times\int_0^\eta\frac{\rho u^2}{\rho_e u_e^2}d\eta-\left(\frac{2\delta}{R}\frac{d\delta}{dx}+\frac{\delta^2}{\rho_e u_e^2 R}\frac{d\rho_e u_e^2}{dx}\right)\times\int_0^\eta\eta\frac{\rho u^2}{\rho_e u_e^2}d\eta-\left(\frac{d\delta}{dx}+\frac{\delta}{R}\frac{dR}{dx}+\frac{\delta}{\rho_e u_e}\frac{d\rho_e u_e}{dx}\right)\frac{u}{u_e}\times\int_0^\eta\frac{\rho u}{\rho_e u_e}d\eta+\left(\frac{2\delta}{R}\frac{d\delta}{dx}+\frac{\delta^2}{\rho_e u_e R}\frac{d\rho_e u_e}{dx}\right)\frac{u}{u_e}\times\int_0^\eta\eta\frac{\rho u}{\rho_e u_e}d\eta+\frac{\delta}{\rho_e u_e^2}\times\int_0^\eta\left(1-\eta\frac{\delta}{R}\right)\left(\frac{\partial p}{\partial x}-\frac{\partial T_{xx}}{\partial x}\right)d\eta-\frac{1}{\rho_e u_e^2}\frac{d\delta}{dx}\int_0^\eta\eta\left(1-\eta\frac{\delta}{R}\right)\left(\frac{\partial p}{\partial\eta}-\frac{\partial}{\partial\eta}T_{xx}\right)d\eta+\delta\frac{\partial}{\partial x}\times\int_0^\eta\frac{\rho u^2}{\rho_e u_e^2}d\eta-\frac{\delta^2}{R}\frac{\partial}{\partial x}\int_0^\eta\eta\frac{\rho u^2}{\rho_e u_e^2}d\eta-\delta\frac{u}{u_e}\frac{\partial}{\partial x}\times\int_0^\eta\frac{\rho u}{\rho_e u_e}d\eta+\frac{u}{u_e}\frac{\delta^2}{R}\frac{\partial}{\partial x}\int_0^\eta\eta\frac{\rho u}{\rho_e u_e}d\eta \quad (5)$$

where $\tau=\mu(\delta u/\delta y)-\rho\langle u'v'\rangle$. Equation (5) becomes applicable to two-dimensional flow as $R\to\infty$.

The normal stress, T_{xx}, which appears in Eq. (5), is not known from mean profile data. However, computations which have been made in this study show that its effect is small. In the results shown, the streamwise gradient of T_{xx} has been neglected.

Knowledge is also required of the static pressure distribution in the boundary layer. In many studies of supersonic boundary-layer flow no attempt is made to measure the static pressure variation normal to the wall, even though for some adverse pressure gradient flows the variation may, in fact, be rather large. In most instances the static pressure at the boundary-layer edge may be determined with confidence. If this is done, the normal pressure variation may then be represented in approximate fashion by assuming a linear distribution between the wall static pressure and the pressure at the boundary-layer edge. Results are shown here for both a linear static pressure distribution and a constant static pressure.

Examination of Eq. (5) shows that an accurate value of boundary-layer growth rate is very important for the calculation of the shear stress. However, precise determination of the boundary-layer thickness from experimental mean data is difficult. It is even more difficult to evaluate the boundary-layer growth rate accurately. This problem may be avoided by using the condition that the shear stress diminishes to zero at the boundary-layer edge and solving Eq. (5) for $d\delta/dx$:

$$\frac{d\delta}{dx}=\left[\frac{C_f}{2}+\left(\frac{\delta}{\rho_e u_e^2}\frac{d\rho_e u_e^2}{dx}+\frac{\delta}{R}\frac{dR}{dx}\right)\times\int_0^1\frac{\rho u^2}{\rho_e u_e^2}d\eta-\frac{\delta^2}{\rho_e u_e^2 R}\frac{d\rho_e u_e^2}{dx}\times\int_0^1\eta\frac{\rho u^2}{\rho_e u_e^2}d\eta-\left(\frac{\delta}{R}\frac{dR}{dx}+\frac{\delta}{\rho_e u_e}\frac{d\rho_e u_e}{dx}\right)\times\int_0^1\frac{\rho u}{\rho_e u_e}d\eta+\frac{\delta^2}{\rho_e u_e R}\frac{d\rho_e u_e}{dx}\int_0^1\eta\frac{\rho u}{\rho_e u_e}d\eta+\delta\frac{\partial}{\partial x}\times\int_0^1\frac{\rho u^2}{\rho_e u_e^2}d\eta-\frac{\delta^2}{R}\frac{\partial}{\partial x}\int_0^1\eta\frac{\rho u^2}{\rho_e u_e^2}d\eta-\delta\frac{\partial}{\partial x}\times\int_0^1\frac{\rho u}{\rho_e u_e}d\eta+\frac{\delta^2}{R}\frac{\partial}{\partial x}\int_0^1\eta\frac{\rho u}{\rho_e u_e}d\eta+\frac{\delta}{\rho_e u_e^2}\frac{dP_w}{dx}\left(1-\frac{\delta}{2R}\right)+\frac{\delta}{\rho_e u_e^2}\frac{d(P_e-P_w)}{dx}\left(\frac{1}{2}-\frac{\delta}{3R}\right)\Bigg]\Bigg/\left[\frac{2\delta}{R}\int_0^1\eta\frac{\rho u}{\rho_e u_e^2}d\eta-\int_0^1\frac{\rho u^2}{\rho_e u_e^2}d\eta+\int_0^1\frac{\rho u}{\rho_e u_e}d\eta-\frac{2\delta}{R}\times\int_0^1\eta\frac{\rho u}{\rho_e u_e}d\eta+\frac{(P_e-P_w)}{\rho_e u_e^2}\left(\frac{1}{2}-\frac{\delta}{3R}\right)\right] \quad (6)$$

In Eq. (6) a linear pressure variation normal to the wall has been assumed.

If the streamwise gradient of the normal stress is ignored and if the flow is assumed to be locally similar, Eq. (5) reduces to the expression used by Bushnell and Morris[1] in their computation of shear stress.

Before solving for the shear stress from Eq. (5), it is also necessary to know the coefficient of skin friction. This may be obtained by using the wall-wake velocity profile proposed by Sun and Childs.[6] The method of least-squares may be used to fit the wall-wake profile to the experimental mean velocity profiles to provide values of C_f and to provide a smoothed representation of the mean velocity distribution.

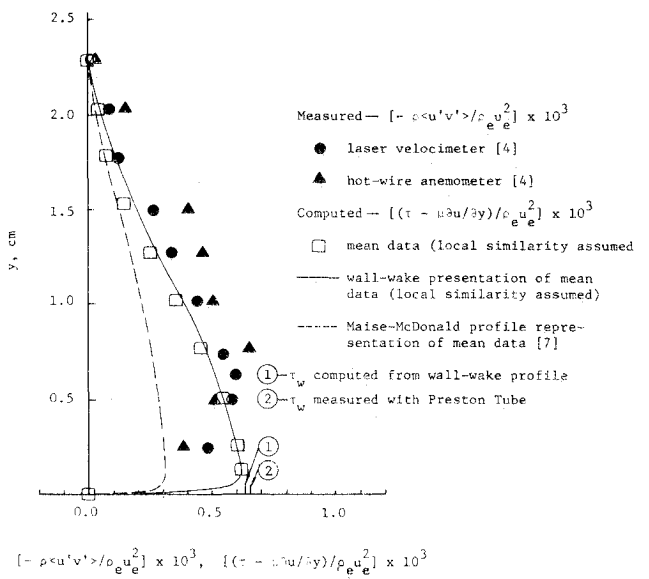

Fig. 1 Turbulent shear stress distribution upstream of a shock-wave boundary-layer interaction, two-dimensional tunnel.[4]

Results

In carrying out the computations for the flow downstream of the shock wave-boundary-layer interactions, the departure from local similarity has been taken into account. For purposes of comparison, however, computations based on local similarity have also been made. The effect of static pressure variation normal to the wall has also been considered for the downstream stations by assuming a linear variation in pressure. In these computations the static pressure at the boundary-layer edge has been computed from the freestream total pressure and pitot pressure with appropriate allowance made for the loss in total pressure across the shock system. The velocity and density profiles needed for the computations were obtained from mean flow pitot profiles with appropriate allowance made for static pressure variation across the boundary layer, and under the assumption of constant total temperature across the boundary layer. As was mentioned in the previous section, the mean velocity profiles may be smoothed by using a least squares fit of the wall-wake velocity profile to the experimental profiles. Computations have been made for both smoothed and unsmoothed profiles.

Figure 1 shows shear stress distributions computed for an upstream ($x = 5.375$ cm) station in Johnson's and Rose's investigation, along with their shear stress data from the hot-wire anemometer and the laser velocimeter measurements. The computed shear values which are shown have been obtained under the assumption of local similarity. As is shown, the calculated results agree quite well over much of the boundary layer with the measured results obtained with the laser veloci-

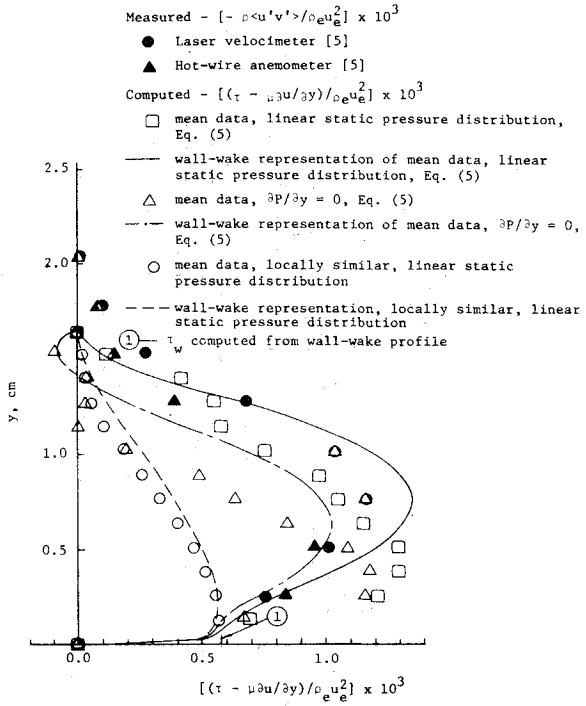

Fig. 2 Turbulent shear stress distribution downstream of a shock-wave boundary-layer interaction, two-dimensional tunnel.[5]

meter. The differences between the calculated results and the hot-wire results are greater. For both the hot-wire and laser velocimeter measurements the peak values of shear stress are seen to occur substantially farther from the wall than is observed for the calculated distributions. Also shown in the figure are values of the wall shear stress as determined by a least squares fit of the wall-wake profile to the mean data and as measured by a Preston tube. The agreement between the two shear stress values is good.

For purposes of comparison, a wall-wake profile proposed earlier by Maise and McDonald[7] has been used to represent the velocity profiles obtained by Rose and Johnson. As is shown, the shear values computed from the Maise-McDonald profile are substantially lower than those obtained with the unsmoothed data or the wall-wake representation described in Ref. 6.

Results of the computations for the data of Rose and Johnson for a station downstream of the shock wave-boundary layer interaction ($x = 9.375$ cm) are shown in Fig. 2 along with their measured shear stress distributions. Several sets of computations have been made from the mean data, including one for purposes of comparison, in which local similarity has been assumed. Results have been obtained for both smoothed and unsmoothed profiles and for both linear and constant static pressure distribution across the boundary layer. The velocity and density profiles used in computing the shear stress are shown in Fig. 3 along with the wall-wake representations of the velocity profiles.

As is shown in Fig. 2, the measured shear stress values obtained by the two experimental techniques are in quite good agreement. These in turn agree reasonably well with the computed values obtained by using smoothed nonsimilar profiles and the assumption of a linear pressure variation across the boundary layer. There is considerable difference between the results for the smoothed and unsmoothed profiles, with the peak shear stress value for the unsmoothed profile occurring lower in the boundary layer. Near the wall the difference apparently was due primarily to inaccuracy in the numerical integration process for the unsmoothed data. Much smaller step sizes could be used with the smoothed data. The results obtained from the wall-wake profiles are valid, of course, only if the profiles provide accurate representations of the actual velocity distributions. In the outer part of the boundary layer, the wall-wake profile provided an excellent representation of the data at one station but did not fit so well at the other. This would account for some of the difference in computed shear stress for smoothed and unsmoothed profiles in that region.

The computed shear values are quite sensitive to the assumptions regarding static pressure. The computed values of static pressure at the boundary-layer edge at the first and second measuring stations differed from those at the wall by 3.0 and 1.2%, respectively. As is shown, the computed values of shear stress with no consideration given to the pressure difference across the boundary layer were substantially lower than those obtained when the pressure difference was considered.

As is also shown in Fig. 2, the results obtained under the assumption of local similarity are markedly different from those determined when similarity is not assumed. The peak shear stress levels computed assuming local similarity are less than half the values computed when similarity is not assumed. Furthermore, the shapes of the shear stress distribution curves are quite different. These results occur even though the differences between profiles at two closely spaced stations are small. The density and velocity profiles in Fig. 3 were obtained at streamwise stations located approximately one boundary-layer thickness apart. Although the profiles at successive stations appear at first glance to be quite similar, striking differences are found for the computed shear stress distributions.

Conclusions

An alternative method of computing shear stress distribution from experimental mean profile data in compressible turbulent boundary-layer flow has been developed. The method is different from those previously reported in that integrated mass and momentum flux profiles and differentials of these integral quantities are used in the computations so that local evaluation of the streamwise velocity gradient is not necessary. The method has been found to yield results which are in reasonably good over-all agreement with directly measured turbulence data for two-dimensional adiabatic boundary layer flow in the regions upstream and downstream of an oblique shock wave interaction. The computed results are quite sensitive to the accuracy of the numerical integrations required in the computational procedure and to the mean property distributions in the boundary layer. The assumption of local similarity may cause large errors in computed shear stress values for flows subjected to pressure gradients, even though adjacent profiles of the mean properties may appear, on first examination, to be quite similar. The computed shear stress levels are quite sensitive to the static pressure distribution normal to the wall. Thus, if reliable shear stress distributions are to be obtained from mean profile data, the static pressure distribution must be known rather accurately.

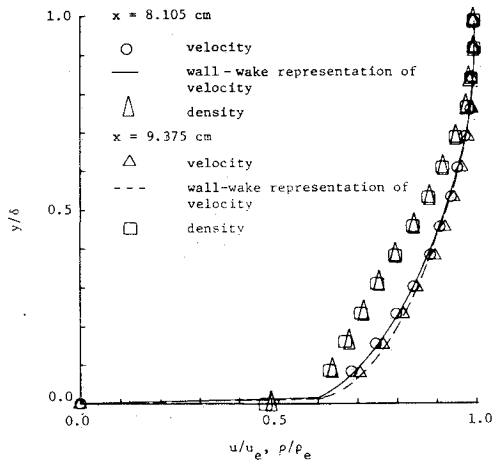

Fig. 3 Density and velocity profiles downstream of a shock-wave boundary-layer interaction.[5]

The effect of the streamwise gradient of the normal stress on the computed results is small and apparently may be neglected.

References

[1] Bushnell, D. M. and Morris, D. J., "Shear-Stress, Eddy-Viscosity and Mixing Length Distributions in Hypersonic Turbulent Boundary Layers," TMX-2310, Aug. 1971, NASA.

[2] Horstman, C. C. and Owen, F. K., "Turbulent Properties of a Compressible Boundary Layer," *AIAA Journal*, Vol. 10, No. 11, Nov. 1972, pp. 1418–1424.

[3] Sturek, W. B., "Calculations of Turbulent Shear Stress in Supersonic Turbulent Boundary-Layer Zero and Adverse Pressure Gradient Flow," AIAA Paper 73-166, Washington, D.C., 1973.

[4] Johnson, D. A. and Rose, W. C., "Measurement of Turbulent Transport Properties in a Supersonic Boundary-Layer Flow Using Laser Velocimeter and Hot Wire Anemometer Techniques," AIAA Paper 73-1045, Seattle, Wash., 1973.

[5] Rose, W. C. and Johnson, D. A., "A Study of Shock Wave Turbulent Boundary-Layer Interaction Using Laser Velocimeter and Hot Wire Anemometer Techniques," AIAA Paper 74-95, Washington, D.C., 1974.

[6] Sun, C. C. and Childs, M. E., "A Modified Wall-Wake Velocity Profile for Turbulent Compressible Boundary Layers," *Journal of Aircraft*, Vol. 10, No. 6, June 1973, pp. 381–383.

[7] Maise, G. and McDonald, H., "Mixing Length and Kinematic Eddy Viscosity in a Compressible Boundary Layer," *AIAA Journal*, Vol. 6, No. 1, Jan. 1968, pp. 73–80.

Effects of Discontinuities in Cylindrical Tubes on a Transmitted Pulse

JOSEPH L. ROSE*
Drexel University, Philadelphia
AND
ARIE BLUM†
Catalytic, Inc., Philadelphia, Pa.
AND
RICHARD W. MORTIMER‡
Drexel University, Philadelphia, Pa.

Nomenclature

L = length of the area discontinuity
λ = pulse wavelength
σ_T = transmitted stress measured at position X_2
σ_I = incident stress measured at position X_1
A_1 = larger cross-sectional area
A_2 = reduced cross-sectional area

Introduction

THE literature on the effects of discontinuities in cylindrical shells is rather limited. Several investigators[1,2] have considered the effects of shells with discontinuous areas on acoustic transmission. The free vibration of a thin cylindrical shell with a discontinuity was studied by Warburton and Al-Mojafi.[3] The effects of discontinuity in bars was studied by Ripperger and Abramson[4] and Kenner and Goldsmith,[5] where the ratio of the transmitted to incident stress was related to the geometrical properties of the bar before and after the discontinuity. In a recent paper, Mortimer, Rose, and Blum[6] obtain a similar relationship between the transmitted to incident stress and the geometrical properties before and after the discontinuity for shells. The analytical results were obtained by numerically solving a general bending shell theory and the results were experimentally verified. This approach was further developed by Rose and Mortimer[7] to obtain a relationship between the transmitted to incident stress in cylindrical shells consisting of a double area discontinuity. The experimental and analytical results obtained in Ref. 7 were in good agreement. However the discontinuity and the pulse duration were rather long. For short discontinuity ($L < \lambda/2$), the effect of the discontinuity on the transmitted pulse is more apparent and the pulse length is more significant. The effects of the pulse length on the propagating pulse in cylindrical shells was recently studied by Mortimer and Blum,[8] and it was shown to be a major parameter in determining the shell response to impact loading.

In this Note the effects of relatively long and short discontinuities are studied. For a relatively long discontinuity ($L \geqq \lambda/2$) a good agreement between experimental results, using ultrasonic technique, and analytical results using the equation developed in Ref. 7, is observed. However, for a relatively short discontinuity ($L < \lambda/2$) due to reflections off the discontinuities, superposition of the wave is now present, which makes the transmitted wave differ in both magnitude and shape from the incident wave. The equation developed in Ref. 7 is no longer valid. Thus, a computer program MCDU-26[6] was used to solve the set of governing equations. Because the frequency of the input pulse is now a function of the magnitude of the transmitted pulse, one computer run was needed to solve the problem for each input frequency. However, if a pulse whose spectral representation consists of a broad range of frequencies is used as input in MCDU 26, and the Fourier series of the transmitted pulse is taken, we now have not only the magnitude of the transmitted pulse of the frequency of the input, but also the magnitudes of the transmitted pulses of all the frequencies that represent the input pulse in the Fourier series. Design curves of various analytical models can be drawn relating frequency to the magnitudes of the incident and transmitted pulses. To check the accuracy of this technique, full sine continuous waves of various frequencies were input pulses to MCDU 26, and the magnitudes of incident and transmitted pulses from these runs showed good agreement to those generated from the design curves.

Investigation and Procedures

The study presented in this Note can be grouped into three investigations. Several experimental and analytical models containing area discontinuities were used. The purpose of the study was to investigate the effects of a relatively long and short discontinuity on the magnitude of the transmitted pulse in a cylindrical tube. This pulse can be related to a stress pulse transmitted through the discontinuity and for clarity in comparison will be referred to hereafter as the magnitude of the transmitted stress.

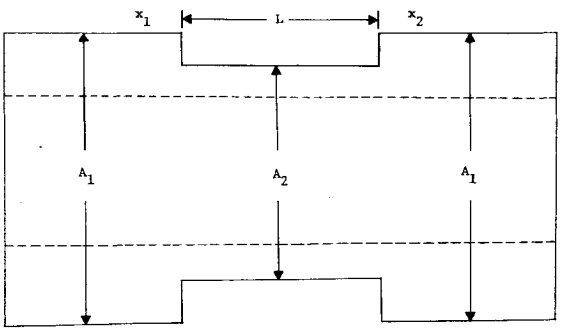

Fig. 1 Schematic of test model.

Received April 12, 1974; revision received August 19, 1974. This work is partly supported by the U.S. Air Force Office of Scientific Research, Arlington, Va.

Index category: Structural Dynamic Analysis.

* Associate Professor of Mechanical Engineering.
† Research Engineer, Catalytic, Inc.
‡ Associate Professor of Mechanical Engineering. Member AIAA.